**NURETH14-628** 

### ASSESSMENT WITH COUPLED THERMO-MECHANICAL CREEP ANALYSIS OF COMBINED CRGT AND EXTERNAL VESSEL COOLING EFFICIENCY FOR A BWR

#### Walter Villanueva, Chi-Thanh Tran\*, and Pavel Kudinov

Division of Nuclear Power Safety, Royal Institute of Technology (KTH), Stockholm, Sweden \*Present address: Institute of Energy, 6 Ton That Tung, Dong Da, Hanoi, Vietnam

#### **Abstract**

In this paper we consider in-vessel stage of a severe core melt accident in a Nordic design Boiling Water Reactor (BWR). Decay-heated pool of corium melt inflicts thermal and mechanical loads on the lower-head vessel wall. Performed thermo-mechanical creep analysis identified two different modes of vessel wall failure: (i) a 'ballooning' of the vessel bottom and (ii) a 'localized creep' concentrated within the vicinity of the top surface of the melt pool. Next, given the mechanical and thermal loads from the decay-heated melt, external vessel cooling is applied at a specified time. It is found that combined CRGT and external vessel cooling was able to suppress the creep and subsequently prevent vessel wall failure.

#### Introduction

Ultimate success of the severe accident management (SAM) strategy in Nordic type Boiling Water Reactors (BWR) is contingent on effectiveness of ex-vessel melt coolability and absence of energetic steam explosion in a deep water pool located under the reactor vessel. When melt is ejected from the reactor pressure vessel, it is assumed that it will fragment, quench, and form a porous debris bed. But the resulting properties of the debris bed, that affect coolability of the bed ([1], [2], [3], [4], [5]) and potential for steam explosion [6], depend significantly on the mode of vessel failure (rupture size and location, characteristic time of melt release from the vessel, temperature and composition of the melt, amount of melt ejected at the first instant, etc.). In general, uncertainties in the ex-vessel melt behavior are largely due to uncertainties in the melt ejection characteristics which are determined by the phenomena of in-vessel stage of the accident and vessel failure. Therefore, in order to establish on a firm basis that containment integrity can be preserved, it is necessary to reduce uncertainties in the modes of vessel failure.

The goal of the present study is to clarify if coolant flow in Control Rod Guide Tubes (CRGT) and ex-vessel cooling can aid in reducing of uncertainties in the vessel failure mode of Nordic type BWRs. Timing of the accident progression and implementation of SAM measures is considered as a key factor in defining success of the in-vessel melt retention. Specifically, the focus of the study is to identify the mode and timing of vessel failure which will also set the time allotted for activation of external vessel cooling e.g. by pumping water into the deep reactor cavity up to the level of the vessel lower head.

The concept of In-vessel Melt Retention (IVMR) has been proposed and developed by Theofanous and coworkers [7]. Several existing designs of Light Water Reactors (LWRs),

Elmir I **Forma** Elmir L **Delete** Elmir L **Delete** Elmir L Delete Elmir L **Delete** Elmir L Delete Elmir L **Delete** Elmir L **Forma** Elmir L **Forma** Elmir L **Forma** 

> Elmir L Forma

Elmir L Forma

such as the Loviisa VVER in Finland and the AP600 and AP1000 incorporated IVMR as part of their severe accident management strategy. Retention of decay-heated melt inside the Reactor Pressure Vessel (RPV) is contingent upon the ultimate mechanical strength of the vessel structures under given mechanical and thermal loads. The mechanical load depends on several factors such as weight of relocated corium, weight of the vessel wall structures and instrumentation attached to the reactor lower head, and vessel internal pressure. While weight of the reactor vessel structures is fixed, the amount of relocated corium to the lower head and internal vessel pressure are subject to accident progression scenario. Nordic-type BWRs adopt a reliable system for depressurization of the vessel in case of core melt accident to reduce the risk related to high pressure melt ejection. The amount of relocated melt to the lower head is determined by the core degradation process which can be slowed down if early activation of cooling by CRGT flow is provided. Detailed investigation on how much reduction of relocated melt mass can be achieved with CRGT cooling is beyond the scope of the present work. Instead we consider how much the transient thermal load on the vessel wall can be reduced by different cooling measures. First, there is a forest of Control Rod Guide Tubes (CRGTs) in the lower head of the BWR. CRGT purge flow can be used as a means for cooling of the formed debris bed (melt pool). Second, there is a hypothetical possibility to fill the reactor cavity with water and cool the RPV external surface. Activation of such additional cooling measure requires considerable time for filling of the deep reactor cavity. The mass of relocated corium is considered as an uncertain parameter in this study. Possibility of in-vessel retention and dependency of vessel failure mode on the amount of the melt in the lower head are studied parametrically.

In the present paper, a coupled thermo-mechanical creep analysis of the RPV is performed to evaluate the effectiveness of the cooling measures for the in-vessel melt coolability and retention. Previously, a thermo-mechanical creep analysis has been performed in 2D geometry for the FOREVER experiment (a scaled model of a Pressurized Water Reactor) [8]. The focus was the prediction of fracture time and location in a vessel under high pressure and with an internally heated melt pool. Another study [9] addressed different failure mechanisms of vessel lower head in a Finnish BWR by a 2D thermo-mechanical analysis. One of the objectives of the study was to analyze different potential failure locations. Previous work by Rempe et al. [10] also addressed different failure mechanisms in PWR and BWR lower heads. They performed structural analyses for the metallic and ceramic debris cases and found that vessel failure will not occur in the metallic debris case within 24 hours but vessel failure is predicted in the case of ceramic debris by localized thinning in the bottom of the vessel in less than 4 hours after debris relocation. In the present work the analysis is performed for the Nordic design BWR lower head with and without external vessel cooling at different melt pool depths. Deformation of the vessel wall are assumed to have negligible effect on the melt pool heat transfer, therefore only one way coupling is employed. Debris bed heatup, remelting, melt pool formation, and heat transfer are predicted with the Phase-change Effective Convectivity Model (PECM) [11]. The PECM is implemented on the platform of the Fluent code [12], and transient heat transfer characteristics are provided for thermo-mechanical strength calculations. The creep analysis is performed using commercial code ANSYS [13], taking into account both the thermal and integral mechanical loads on the RPV. Material properties of the reactor vessel [10] are used as an input data for the creep analysis. Results of coupled simulations and appropriate integrated schemes for in-vessel coolability and retention are discussed in detail.

Elmir L Forma Elmir L Delete

In the next section, thermal and mechanical aspects of the analysis including the creep modeling are given. In Section 2, results of four cases with different melt pool depths are presented and discussed. In addition, the possibility of in-vessel retention with CRGT and external vessel cooling is investigated.

#### 1. Computational treatment

First, transient formation of the melt pool and thermal load from the melt pool to the vessel wall is calculated with the PECM (that is implemented in Fluent). Then, the coupled thermo-mechanical creep analysis of the reactor pressure vessel is implemented in ANSYS with imposed distributions of internal and external vessel walls temperatures predicted by PECM.

#### 1.1. Thermal and mechanical aspects

#### 1.1.1. <u>Material properties</u>

We consider the vessel to be made of steel SA533B1 with material properties such as density, elastic modulus (linear isotropic), thermal conductivity (isotropic), specific heat, and coefficient of thermal expansion (that are all functions of temperature) are taken from Rempe et al. [10]. The Poisson's ratio is set to 0.3. We note that the elastic modulus is highly dependent on temperature, which decreases 2 orders of magnitude as the temperature increases from 300 to 1050 K. Consequently, the strain due to creep increases significantly at high temperatures as the elastic response of the material is inversely proportional to the elastic modulus.

## Elmir L Elmir L Forma

#### 1.1.2. Axisymmetric model geometry and mesh

The geometry considered for the structural analysis is a 2D axisymmetric model of a Nordic design BWR, see Figure 1.

The element type used in ANSYS 12.1 [14] is Quad Plane223 which is a 2D 8-nodecoupled-field (structural-thermal) solid. For full transient analyses, a strong structural-thermal coupling is supported. The 2D geometry is meshed with 800 quadrilateral elements and 2731 nodes with an average edge length of 0.04 m. A typical run with this mesh and a time-step of 10 s on an Intel Core 3GHz Linux platform takes about 0.78 h. But for the case with external cooling, the time-step is reduced to 1 s from the start of cooling in order to resolve the rapid changes in heat flux on the outer surface of the vessel wall.

## Elmir L Forma Elmir L Delete

#### 1.1.3. Boundary conditions and other input parameters

Mechanical strength of the vessel wall depends on the thermal loads imposed on its boundaries. In the present work the Effective Convectivity Model (ECM) is used for prediction of transient thermal loads imposed on the vessel wall from a decay-heated debris bed and melt pool formed in the BWR lower head during a severe accident. The ECM has been developed based on the concept of effective convectivity which was pioneered by Bui and Dinh [15]. The ECM is a model for description of turbulent natural convection heat transfer in an internally heated fluid volume. In the ECM method, the convective terms of the energy conservation equation are described using characteristic velocities; therefore the need of solving Navier-Stokes equations is eliminated [11]. The characteristic velocities are determined using experimental heat transfer correlations, namely the upward, sideward and downward Steinberner-Reineke correlations [16]. The ECM is implemented in the

commercial code Fluent, to utilize all advantages of a CFD commercial code solver such as the pre- and post-processing.

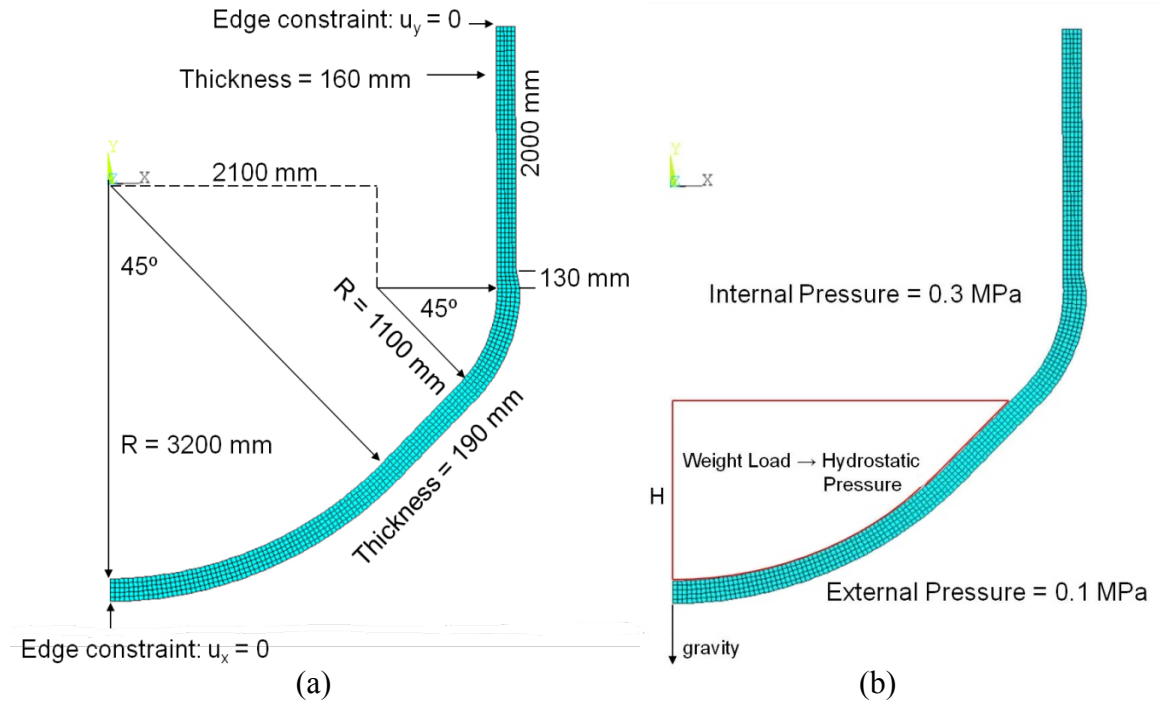


Figure 1. (a) 2D axisy nodes, an

ic geometry and mesh with 850 quadr chematics of mechanical load on the 1 l elements and 2901 vessel.

To describe the crust ion phenomer (PECM). The ECM an a broad spectrum of please wide range of Rayleigh accurate and computat transfer for a BWR accurate ion phenomera may be in the ECM and the second in the seco

ion phenomena, the ECM was exten M have been validated against a set continuous phenomena involved in melt pool former. The ECM and PECM have been conficient tools for 3D simulations of unalysis [17].

Phase-change ECM riments which cover on heat transfer, and strated as sufficiently pool formation heat

In the present work PECM simulations are performed for a 3D slice of BWR lower plenum. The slice geometry is a segment of BWR lower plenum including 6 cooled CRGTs, filled with decay-heated corium, and bounded from below by the vessel wall. It is assumed that a debris bed is formed in the lower plenum, due to inadequate cooling the debris bed is heated up and remelted. In this work we assume that the Instrumentation Guide Tubes (IGTs) are melted and plugged by corium melt during gradual remelting of the debris, and do not have an influence on melt pool heat transfer. The CRGTs are cooled from inside by water flow. The water is assumed to be ejected from the CRGTs providing a water layer atop of the debris bed. Two cases are considered in the present paper; in the first case, the maximum debris bed thickness is 0.7 m, and in the second case the maximum bed thickness is 1.0 m. The boundary conditions applied for the simulation cases are as follows. The top and CRGTs walls are applied to Dirichlet boundary conditions, i.e. isothermal with water saturation temperature. Other surfaces are applied to Neumann boundary conditions. The external surface of the vessel wall is covered with insulation therefore a small heat flux (20 W/m<sup>2</sup>) is allowed. In the cases where effect of the external vessel wall cooling is studied this boundary condition is changed instantaneously to Dirichlet boundary condition with water saturation temperature once external cooling is applied. Resulting transient thermal loads on the vessel wall are then used for the thermo-mechanical creep analysis.



A snapshot of the temperature and melt fraction for H = 0.7 m debris bed at t = 4.44 h is shown in Figure 3. The debris bed is surrounded by cooled CRGTs so higher level of temperature can be seen in-between CRGTs and consequently melt forms first in these regions. The volume averaged temperature at this time is about 2367 K while the volume fraction of the liquid melt is around 0.5. Figure 5, shows the temperature and liquid melt fraction for H = 1.9 m debris bed at t = 3.47 h. In comparison to the 0.7 m case, the cooled CRGTs are not evenly placed in the space occupied by the melt and there is a significant region on the upper end where melt forms faster than in the rest of the debris bed. At this time the volume fraction of liquid melt is around 0.3 and the volume averaged temperature is about 2386 K.





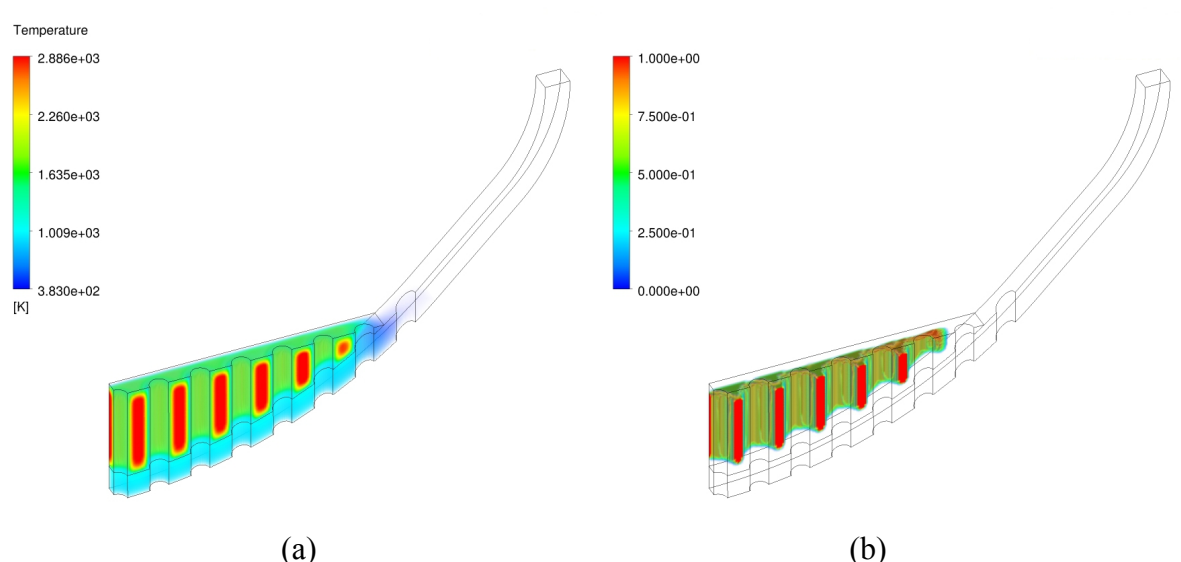


Figure  $\underline{3}$ , (a) Temperature profile at t = 4.44 h for H = 0.7 m debris bed, and (b) corresponding melt fraction.



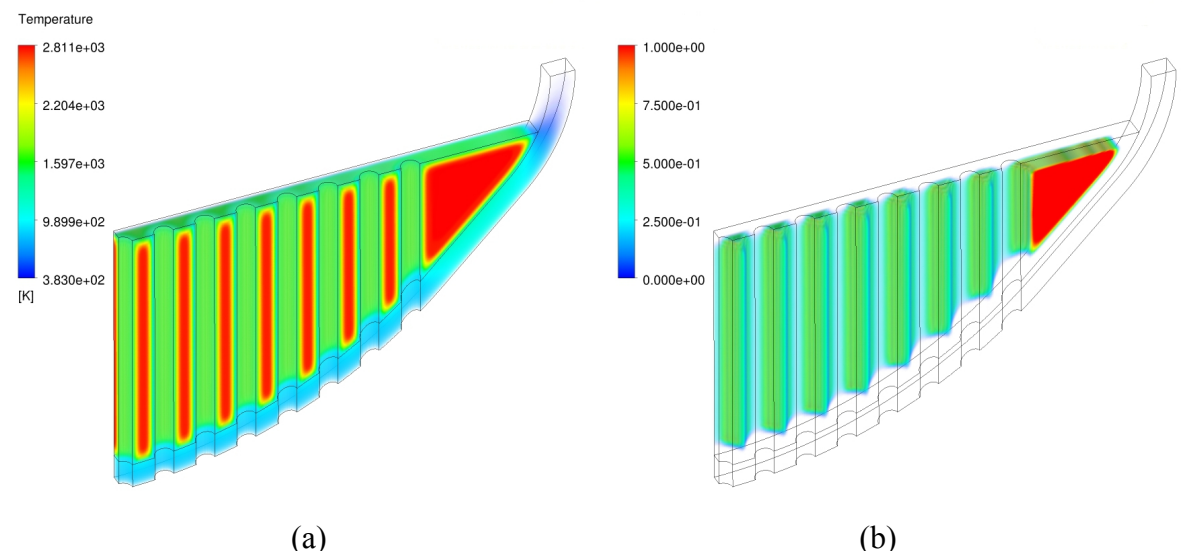


Figure 5. (a) Temperature profile at t = 3.47 h for H = 1.9 m debris bed, and (b) corresponding melt fraction.



#### 1.2. Creep model and validation

In this section, we provide description of the creep model and parameters used in the

calculation as well as the curve fitting of the experimental creep data. We will show in the next section the importance of including the creep analysis in the calculation, as creep is considered the main cause of failure of the reactor pressure vessel given the above mechanical and thermal loads, especially with the high temperature load on the internal vessel as a result of melt pool formation.

It is well known that stress and temperature can affect significantly the creep rate of structural materials. A typical creep curve consists of three stages before rupture, namely, the primary stage (also called transient creep), secondary (steady creep), and tertiary (accelerating creep). They correspond to a decreasing, constant, and increasing strain rates, respectively [18]. A single equation (or model) cannot capture all the stages of the creep curve of a given material. To add more to its complexity, there are different creep curves for different temperatures and stresses, i.e., the creep strain is a function of time, temperature, and stress.



For our analysis, a modified time hardening (primary) creep model is chosen in ANSYS,

$$\varepsilon_{cr} = \frac{c_1 \sigma^{c_2} t^{c_3 + 1}}{c_3 + 1}, \qquad c_1 > 0,$$
 (1)

where  $\varepsilon_{cr}$  is the equivalent creep strain,  $\sigma$  is the equivalent stress, t is time, and  $c_1$ ,  $c_2$ , and  $c_3$  are constants to be determined by curve fitting with experimental data. Using the experimental creep data for SA533B1 from Rempe et al. [10], the coefficients, as summarized in Table 1, are generated for different temperatures. An example of the ANSYS creep model validation at temperature T = 1150 K with a stress of 26.5 MPa is given in Figure 7.

Table 1. Coefficients of the modified time hardening given in Equation 1 for different temperatures.

| Temperature [K] | 900                     | 1050                    | 1150                    | 1250                    | 1373                    |
|-----------------|-------------------------|-------------------------|-------------------------|-------------------------|-------------------------|
| $\mathbf{c_1}$  | 1.461×10 <sup>-31</sup> | 1.867×10 <sup>-42</sup> | $7.801 \times 10^{-28}$ | 3.497×10 <sup>-44</sup> | 5.383×10 <sup>-47</sup> |
| $c_2$           | 3.0881                  | 4.8171                  | 3.0886                  | 5.5237                  | 6.2092                  |
| c <sub>3</sub>  | -0.0560                 | 0.1609                  | -0.0180                 | -0.1219                 | -0.0554                 |

As a validation test, a uniaxial structural creep analysis was performed with a rectangular block (1 m  $\times$  0.2 m) at constant temperature T = 1150 K, clamped on one end, and applied stress of 26.5 MPa on the opposite end. The time-step (10 s), mesh edge size (0.04 m), and all other relevant input parameters discussed above are also used in the numerical validation. It is found that the standard norm of the difference between the numerical calculation and theory (Equation 1) is 0.4 % strain. Additional tests with uniform mesh edge sizes of 0.1 m and 0.02 m also yielded the same norms of about 0.4 % strain. On the other hand, the norm of the difference between the experiment and theory (Equation 1) is 3.6 % strain. However, considering only the range of reliably predicted (the percent strain within 20 % in Figure 7), the norm of the difference between the experiment and theory is 2.3 %.

In this study, we will not identify a yield or creep limit. This is motivated by the fact that creep is a thermally activated process and the material starts to creep even under moderate stresses lying below the yield limit [19]. In addition, the existence of a creep limit cannot be verified experimentally at high temperatures since the main creep mechanism for metals and







alloys is the diffusion of vacancies [20]. Instead we identify a range of percent strain that we consider as reliably predicted by the model and beyond this range the results are only considered in a qualitative manner, meaning, that failure may happen in this stage but its exact time and respective deformations cannot be accurately determined. We consider strains within 20 % as reliably predicted, which is partly based on the experimental creep data and the primary creep model that we used. The time scale to reach 20 % strain is one of our main interests as this provides the time scale for delay in activation of external cooling.



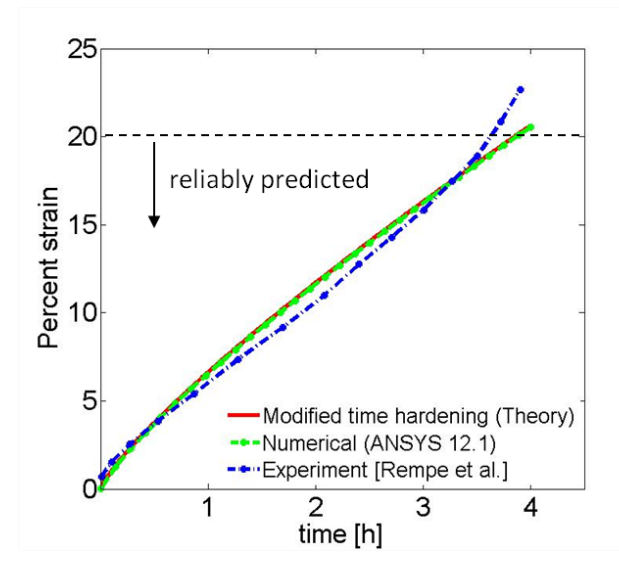


Figure 7. ANSYS creep model validation results for a rectangular block, set at constant temperature, clamped on one end, and an applied stress on the opposite end. The material is SA533B1 steel at T = 1150 K with a stress of 26.5 MPa. The experimental data is taken from Rempe et al. [10] and the ANSYS model is modified time hardening (primary creep) given in Equation 1.

#### Elmir L Delete

#### Elmir L Forma Elmir L Delete

#### 2. Results and discussion

A coupled thermo-mechanical creep analysis of the pressure vessel lower head is performed with different melt pool depths H = 0.7 m, 1.1 m, 1.5 m, and 1.9 m. Two modes of vessel wall failures are observed, namely, (i) 'ballooning' type and (ii) 'localized creep'. Possibility of in-vessel retention is demonstrated when both CRGT cooling and external cooling are applied.

Figure 9 shows the von Mises creep strains and displacements of the vessel wall for the case with melt pool depth H = 0.7 m (about 30 tons of melt). At time t = 4.72 h in Figure 9a, the maximum creep strain has reached 0.018 with maximum displacement of 0.06 m. Then at time t = 4.92 h (Figure 9b), the maximum creep strain has reached 0.19 located along the vicinity of the top of the melt pool while most part of the lower section has creep strains between 0.02-0.17. Furthermore, the maximum displacement at the bottom center of the pressure vessel has become 0.26 m and displacements get smaller as one reaches the top of the pool which indicates a 'ballooning' type of failure. The rest of the vessel has negligibly small displacements. This ballooning mode of failure intensifies in Figure 9c at a later time t = 5.0 h, although, we cannot consider the displacements and creep strains at this time to be reliably predicted since the maximum creep strain has reached 0.39. To demonstrate the importance of inclusion of creep analysis, Figure 9d shows a thermo-mechanical analysis with









the same thermal loading but without creep modeling in mechanical analysis at time t = 5.0 h and the maximum total mechanical and thermal strain has only reached 0.008 with a maximum displacement of 0.05 m. Even at a later time t = 10.0 h, the total mechanical and thermal strain has reached 0.03 and the maximum displacement has become 0.10 m.



Figure 9. (a)-(c) von Mises creep strains and displacements at 4.72 h, 4.92 h, and 5.0 h, respectively, with melt pool depth H = 0.7 m, and (d) Without creep: von Mises total mechanical and thermal strain at 5.0 h. The initial undeformed edges are superimposed. The maximum displacements are (a) 0.06 m, (b) 0.26 m, (c) 0.48 m, and (d) 0.05 m.



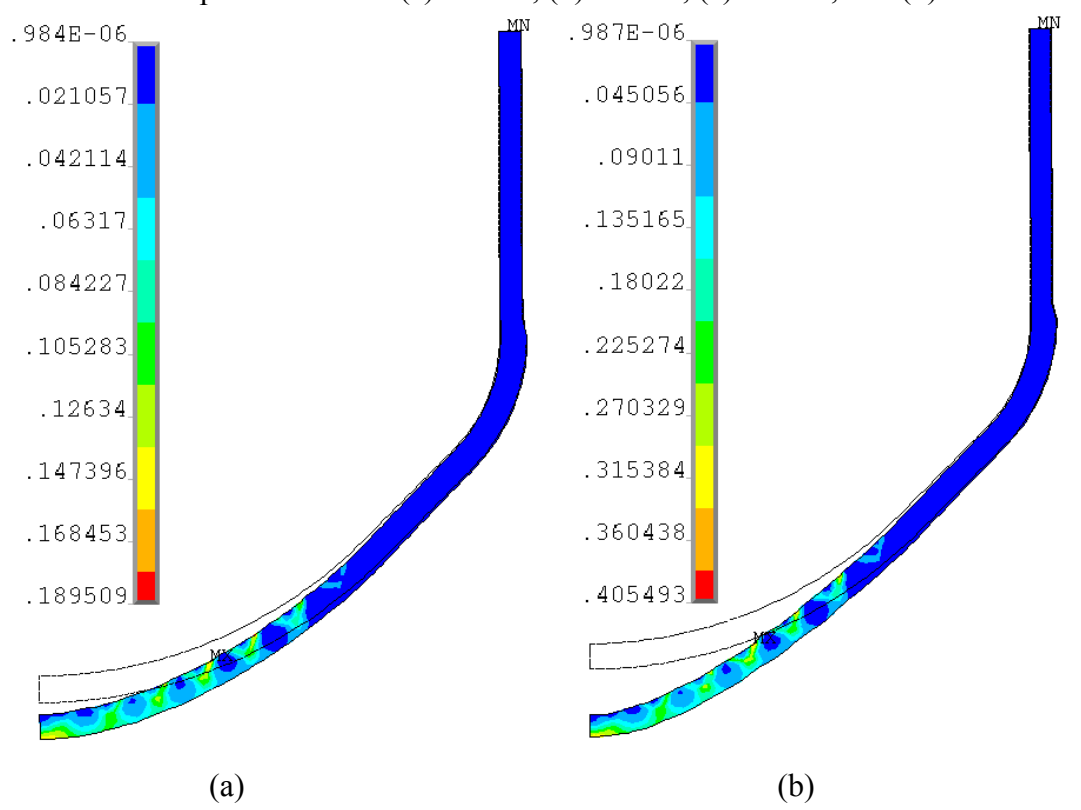


Figure 11, von Mises creep strains and displacements with melt pool depth H = 1.1 m at (a) 4.86 h, and (b) 4.94 h. The maximum displacements are (a) 0.27 m, and (b) 0.52 m.



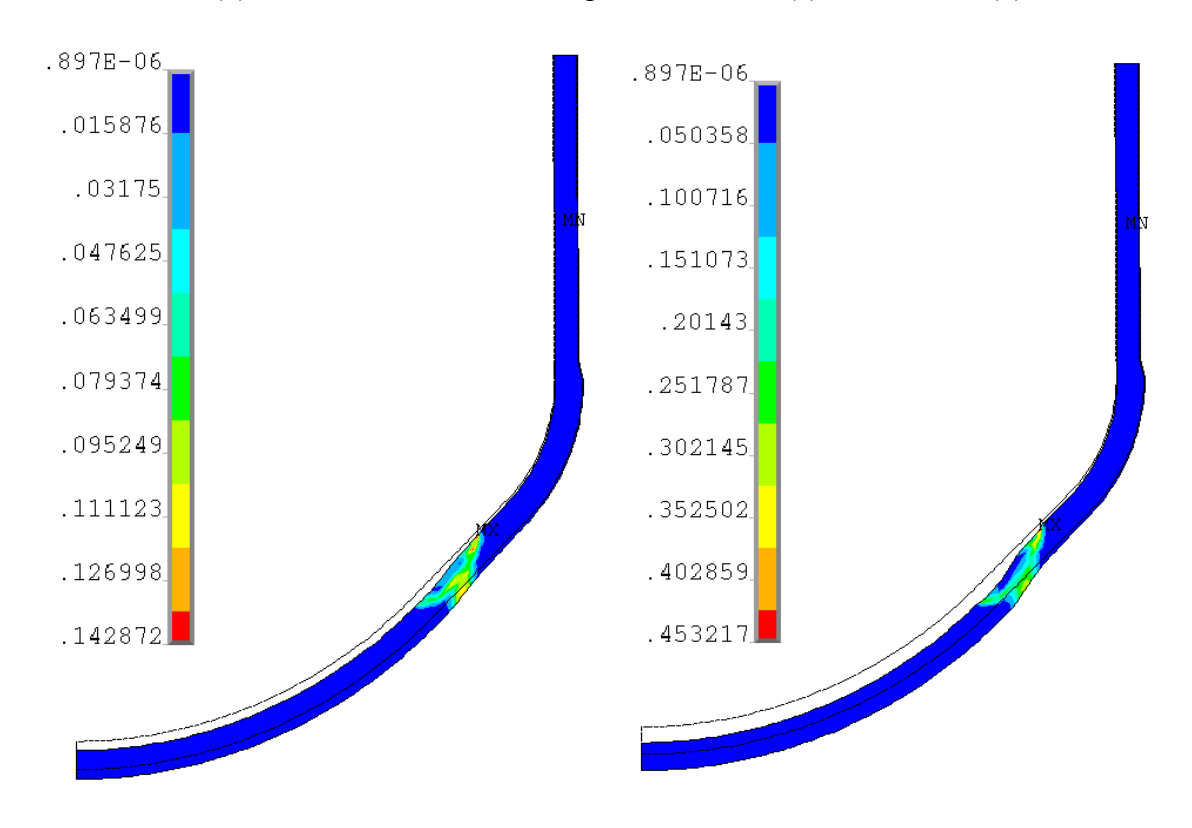




Figure 12, von Mises creep strains and displacements with melt pool depth H = 1.5 m at (a) Elmir L 3.78 h, and (b) 3.89 h. The maximum displacements are (a) 0.06 m, and (b) 0.11 m. **Delete** .797E-06. .799E-06 .001395 .018171 .002789 .036341 .004183 .054511 .005577 .072681 .006971 .090851 .008365 .109021 .009759. .127191 .011153. .145361 .012547 .163531. (a) (b) .800E-06 .073544 .147087 .220629 .294172 .367715. .441258 .514801 .588344 .661887. (c)



is and displacements with melt pool depth H = 1.9 m at (a) with a close-up of the localized creep region. The maximum



displacements are (a) 0.04 m, (b) 0.07 m, and (c) 0.18 m.

In Figure 11, the von Mises creep strains and displacements are shown for the case with melt pool depth H = 1.1 m (about 80 tons of melt). At time t = 4.86 h in Figure 11a, the maximum creep strain has reached 0.19 while the maximum displacement is 0.27 m. The general behavior is similar to the previous case with 0.7 m pool and also can be characterized such as "ballooning" with highest creep strains at the bottom part of the pool. This effect is amplified in the succeeding Figure 11b at a later time t = 4.94 h.

For a deeper melt pool depth H = 1.5 m (about 140 tons of melt), a different mode of failure, namely 'localized creep', is observed where strains are localized in the region right below the pool top surface (Figure 12a). The deformations of the lower part of the vessel are small and displacement is almost uniform at 0.06 m in contrast with the previous ballooning case where bottom part of the vessel was considerably deformed. A similar but more intensified behavior is seen in Figure 12b at a later time t = 3.89 h. Deformations induced by the mechanical load have its maximum at the bottom center but the deformations induced by the thermal load have its maximum at the upper region, therefore resulting in a relatively uniform displacement of the region covered by the melt pool.

At the maximum melt pool depth H = 1.9 m (which corresponds roughly to 200 tons of debris), a localized creep is also observed, as shown in Figure 13a. The maximum von Mises creep strain at time t = 3.19 h is 0.012 with a maximum displacement of 0.04 m. In Figure 13b which corresponds to a later time t = 3.47 h, the maximum creep strain increases to 0.16 with creep strains localized in the region right below the pool top surface. Furthermore, the maximum displacement is 0.07 m and displacements are almost uniform (small deformations) in the region below the localized creep. The same qualitative behavior intensifies at a later time t = 3.61 h as shown in Figure 13c with a magnified view of the localized creep region.

In both 0.7 m and 1.1 m cases, the melt pool covers a region in the lower head where cooled CRGTs are evenly distributed. A relatively uniform thermal load in this cases result in creep strains spread evenly in the vessel region heated by the pool. In combination with a relatively small mechanical load, that is, a melt pool mass below 80 tons, the distributed creep strain accounts for the ballooning type of failure.

In case of 1.5 m and 1.9 m deep pools the outer periphery of the melt pool (beyond the radius of 2.1 m) is not penetrated by cooled CRGTs. Along with the increased natural convection heat flux at the top region of the big pool, this results in a considerably higher temperature of the vessel wall above the height of 1.2 m from the bottom (or above 45°, see Figure 19a for an example). The effect of higher thermal load in the region right below the top pool surface dominates along with the effect of considerably bigger mechanical load (more than 130 tons of melt) changes failure mode to the localized creep. This behavior is consistent with our previous study [21] on a similar design but with smaller vessel lower head. With a 1.0 m debris depth, there exists a region in the outer periphery of the melt pool that is not penetrated by cooled CRGTs, thus changing the mode of failure to localized creep from a ballooning mode in the 0.7 m case.

Figure 9 shows the vertical displacement of the bottom center of the reactor vessel with melt pool depths H = 0.7, 1.1, 1.5, and 1.9 m. The plot is divided into solid lines which represent reliably predicted results and dotted lines which represent beyond reliably predicted strains (results which can be considered only qualitatively). As stated previously, we consider failure

Elmir L Delete

Elmir L Delete

Elmir L Delete

Elmir L Delete

Elmir L Forma and gra Elmir L Delete

Elmir L

Elmir L
Forma
and gri
Elmir L
Forma
and gri

Elmir L

Delete

Elmir L

Forma and gra Elmir L

Elmir L Forma Elmir L Delete



of the global vessel wall to happen when the maximum creep strain goes beyond 20 % but cannot infer exactly the time of failure and the corresponding deformations. However, once the maximum creep strain follows an accelerated increase, failure of the global vessel wall is considered imminent. For melt pool depths of 0.7 m and 1.1 m which shares the same mode of failure, the vertical displacement of their bottom center is almost identical within the reliably predicted range. A rapid increase of relative displacement and acceleration of vessel creep takes place after about 4.47 h. The external cooling of the vessel, in order to be effective in suppressing creep and possibly preventing vessel wall failure, has to be applied prior to this time. The global vessel creep acceleration for the 1.5 m case is earlier at 3.58 h, and earliest at 3.31 h in the 1.9 m case.

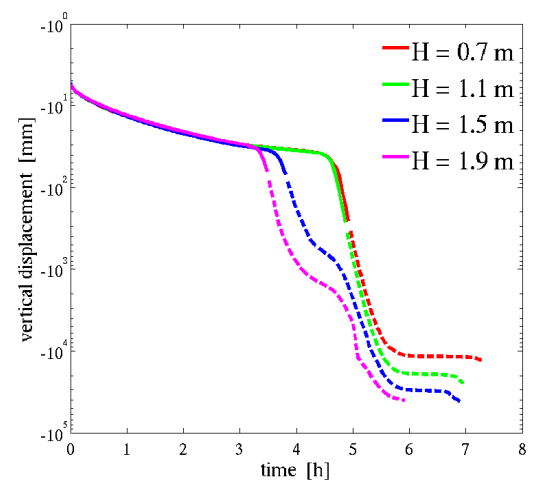


Figure 9. Vertical displacement of the bottom center of the reactor vessel with melt pool depths H = 0.7, 1.1, 1.5, and 1.9 m. The solid lines indicate reliably predicted results that correspond to maximum creep strains within 20 %.

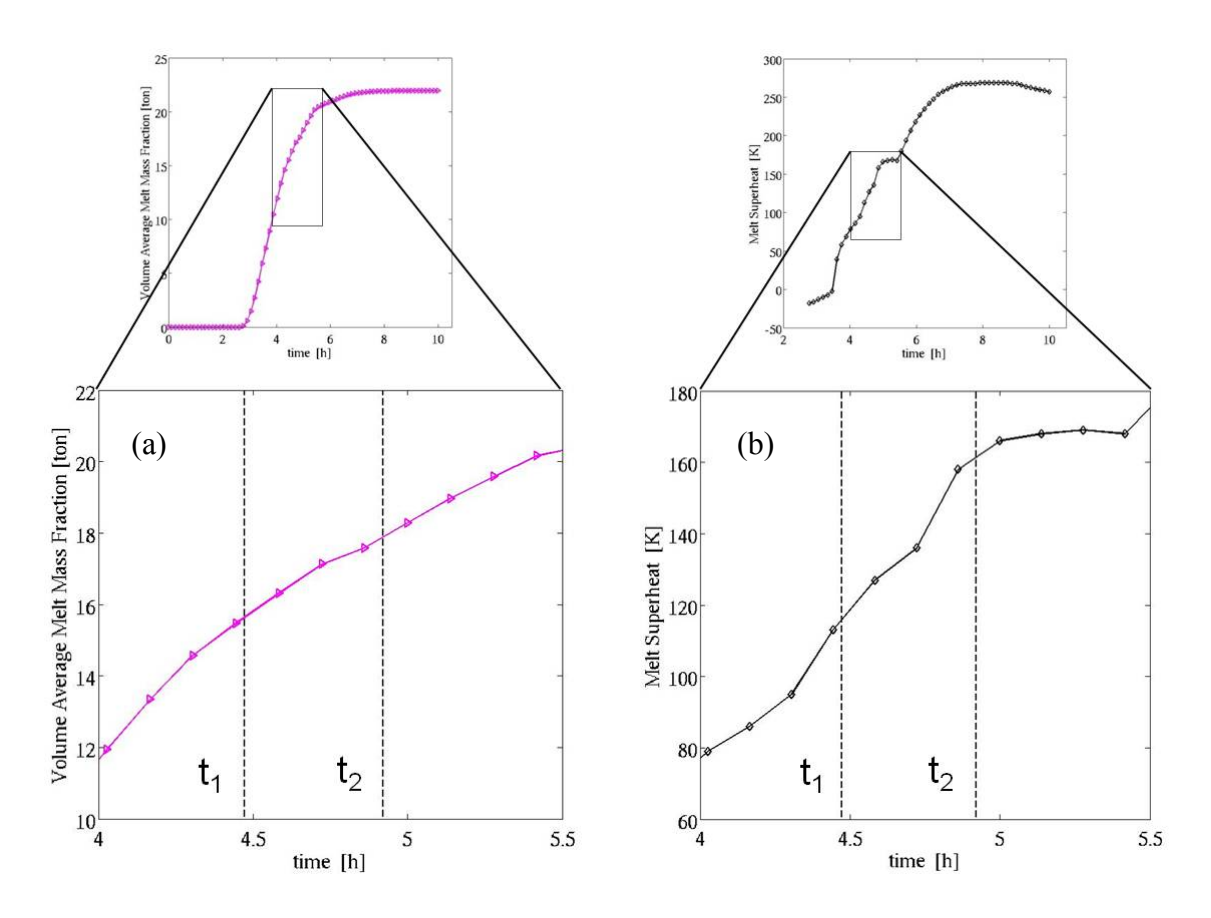


Figure 11 (a) Volume averaged melt mass fraction in the debris bed as a function of time for H = 0.7 m, and (b) corresponding average melt superheat. The timings  $t_1$  and  $t_2$  correspond to the estimated start of creep acceleration and time where 20 % maximum creep strain has been reached, respectively.

Elmir L Delete

From the PECM calculations, Figure 11, shows the volume fraction of liquid melt in the debris bed as a function of time for H = 0.7 m and the corresponding volume averaged superheat of liquid melt. This information can provide a rough estimate of the debris bed conditions in case of a global vessel wall failure, that is, the amount and superheat of the melt that is available for ex-vessel melt release. The two timings  $t_1 = 4.47$  h and  $t_2 = 4.9$  h corresponding to the estimated start of creep acceleration and time where 20 % maximum creep strain has been reached, respectively, are also plotted. The amount of melt at  $t_2 = 4.49$  h is around 18 tons (from the total mass of 30 tons) with an average melt superheat of about 160 K. After 30 min, the amount of melt increases to about 20 tons with an average melt superheat of around 168 K.



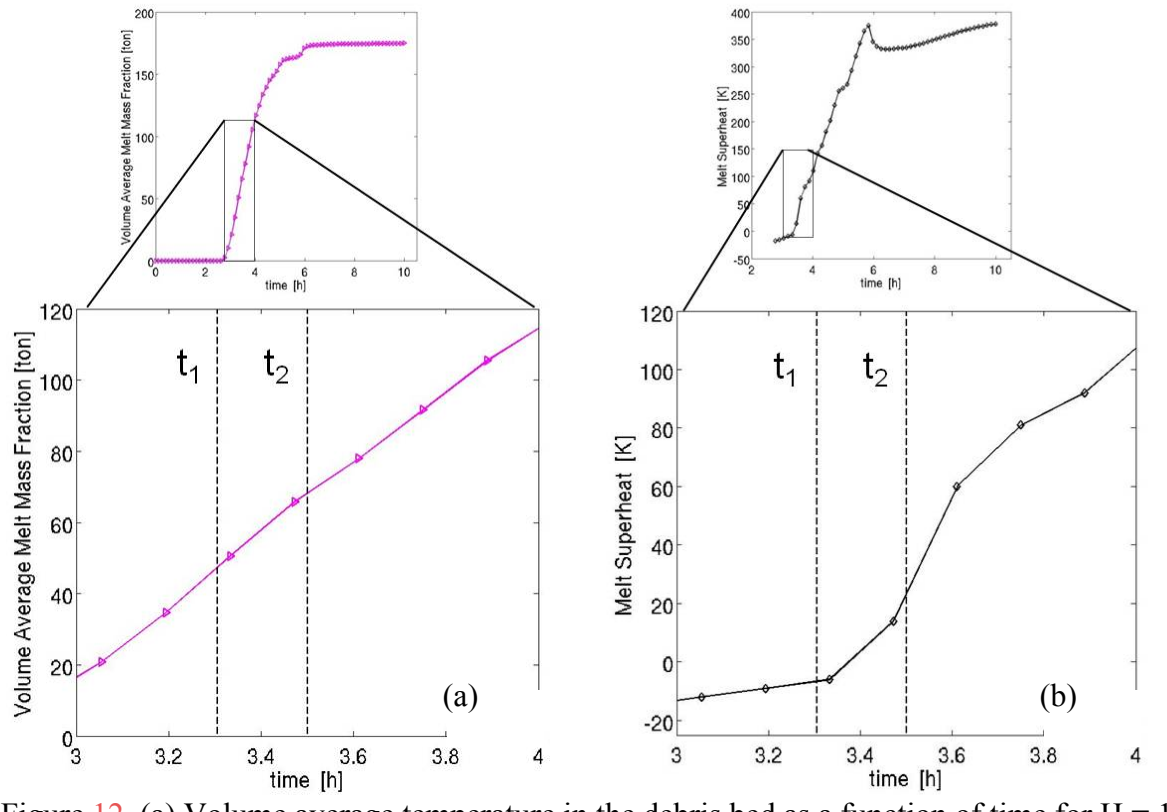


Figure 12 (a) Volume average temperature in the debris bed as a function of time for H = 1.9 m, and (b) corresponding volume average melt fraction. The timings  $t_1$  and  $t_2$  correspond to the estimated start of creep acceleration and time where 20 % maximum creep strain has been reached, respectively.



Table 2. Debris bed conditions at time t<sub>2</sub> where 20 % maximum creep strain has been reached and then after 30 minutes.

| H [m] | Start time of                    | Time at max ~20 %                | Amount of liquid      | Average melt                     |
|-------|----------------------------------|----------------------------------|-----------------------|----------------------------------|
|       | creep                            | creep strain, t <sub>2</sub> [h] | melt at t2 (and after | superheat at t <sub>2</sub> (and |
|       | acceleration, t <sub>1</sub> [h] |                                  | 30 min) [ton]         | after 30 min) [K]                |
| 0.7   | 4.47                             | 4.9                              | 18 (20)               | 160 (168)                        |
| 1.1   | 4.47                             | 4.9                              | 52 (56)               | 187 (232)                        |
| 1.5   | 3.58                             | 3.8                              | 58 (81)               | 72 (139)                         |

| 1.9 | 3.31 3.5 | 68 (112) | 23 (103) |
|-----|----------|----------|----------|
|-----|----------|----------|----------|

Figure 12 shows the debris bed conditions for H = 1.9 m. From the total mass of 200 tons, an estimated 68 tons of melt has formed at  $t_2 = 3.5$  h with an average melt superheat of only 23 K. But after 30 min, the amount of melt rapidly increases to about 112 tons and also with a significant increase in melt superheat to around 103 K. A summary of debris bed conditions for all cases, H = 0.7 m, 1.1 m, 1.5 m, and 1.9 m, is given in Table 2.

Elmir L Delete Elmir L Forma

In all considered cases the results of analysis indicate that vessel failure has to be expected if only CRGT cooling is applied. An important question for accident management is the possibility of in-vessel retention by the means of combined CRGT cooling and ex-vessel cooling. In reality, the timing for activation of ex-vessel cooling (in the event of core damage) depends on many plant design-specifics factors (time necessary to remove vessel insulation and pump the water up to the vessel level, etc.). In this study, we choose the time of external vessel cooling to be right before the beginning of vessel creep acceleration. In both the 0.7 m and 1.1 m cases, this time is 4.44 h, while it is 3.47 h in the 1.5 m and 3.19 h in the 1.9 m case. We assume that the water level at the external cavity pool has instantaneously reached the same level as the melt pool at the specified times. In this work, we use the simplest way to implement such vessel cooling by setting a temperature boundary condition at water saturation temperature, T = 373 K. The effect of external vessel cooling on the vertical displacement of the bottom center of the reactor vessel is shown in Figure 13. Prior to applying of external cooling, the vertical displacements are identical with the previous results (Figure 9). Right after the application of external cooling, the relative vertical displacements in all cases rapidly decrease and two of those cases (shallower pools 0.7 m and 1.1 m) even surpass their initial positions. A check on the displacements of the other parts of the vessel wall also reveals the same behavior.



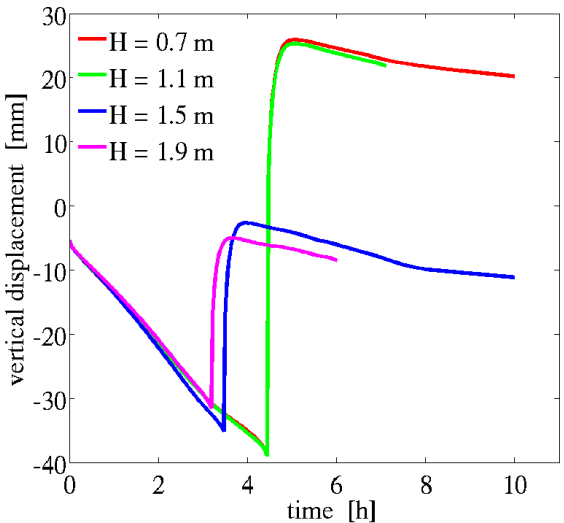
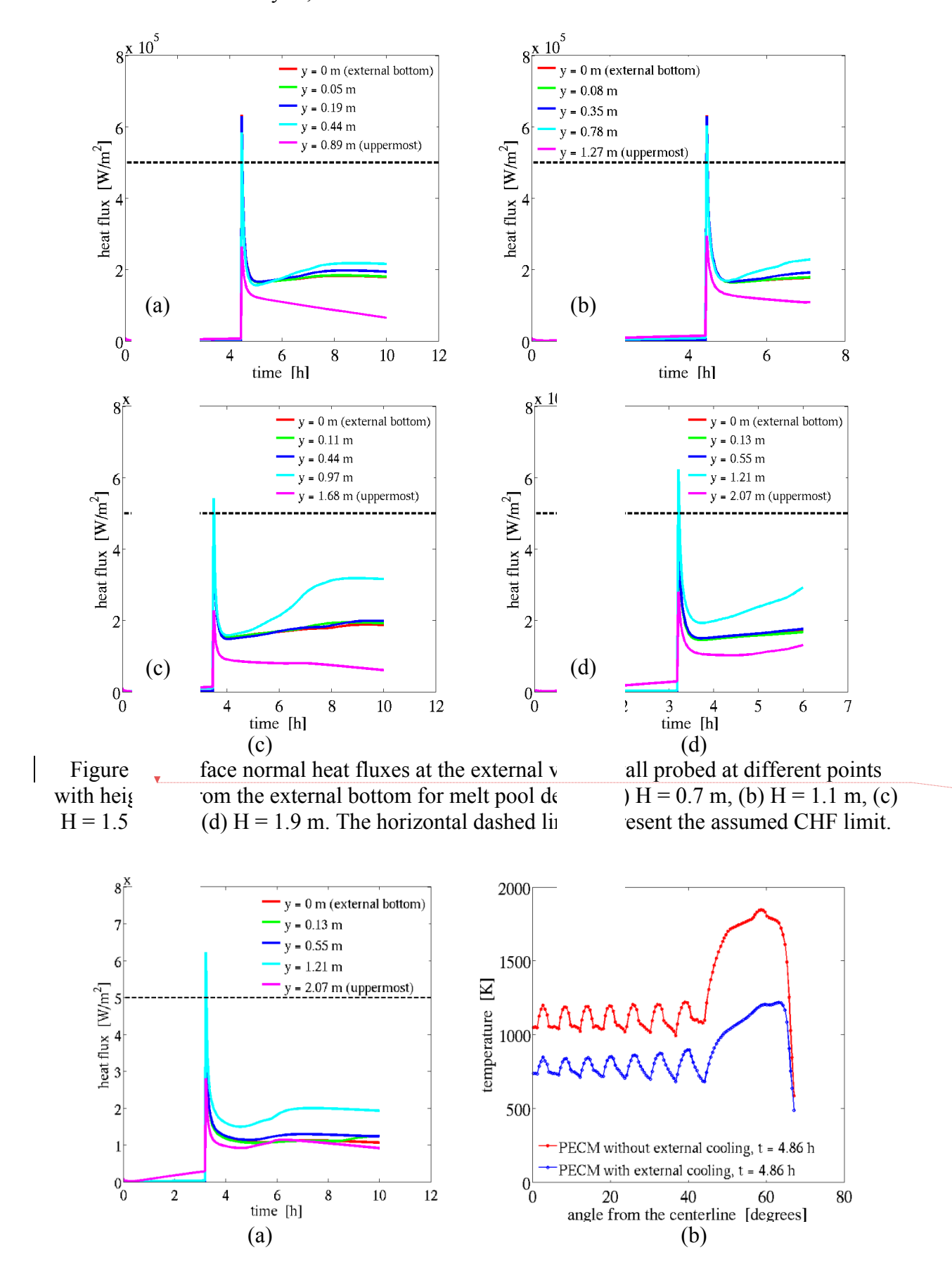


Figure 13. Effect of external vessel cooling; vertical displacement of the bottom center of the reactor vessel with melt pool depths, (i) H = 0.7 m externally cooled at 4.4 h, (ii) H = 1.1 m externally cooled at 4.4 h, (iii) H = 1.5 m externally cooled at 3.47 h, and (iv) H = 1.9 m externally cooled at 3.19 h.



It is known that one of the critical issues in the IVMR provided by external vessel cooling is the avoidance of film boiling regime which is characterized by the critical heat flux (CHF). Previous studies ([22], [23]) have examined the coolability limits of a reactor pressure vessel lower head. They found that the CHF can increase from ~500 kW/m<sup>2</sup> at the very bottom point

of the vessel, up to  $\sim 1000 \text{ kW/m}^2$  on the upper side surface of the vessel wall. For the sake of conservatism in our analysis, we consider the lower bound at  $500 \text{ kW/m}^2$  as a CHF limit.



Elmir L

Delete

Figure 19, (a) Effect of external cooling on the thermal load from the melt pool at a snapshot time t = 4.86 h for H = 1.9 m debris bed. (a) Wall normal heat flux at the external vessel surface for H = 1.9 m debris bed; (b) external vessel wall temperature.

Elmir L Delete

The normal heat fluxes at the external vessel surface probed at different points with depths y from the vessel bottom are shown in Figure 15, for all considered cases. Prior to the corresponding cooling times, the normal heat fluxes are negligible according to the prescribed boundary condition. At the instant of application of external vessel cooling, the normal heat fluxes suddenly peak which is a result of assumed instantaneous changes in thermal boundary condition. In reality, the vessel external surface is initially at temperature higher than the minimum film boiling temperature and its cooling and then rewetting processes are expected to be gradual. The eventual transition from film boiling to nucleate boiling is expected to occur since the steady heat flux is well below CHF, however, how much time this process may take has to be addressed in a separate study.

Forma
Elmir L
Delete

In all cases, the heat flux quickly settles to a level below the conservatively assumed CHF limit of  $500 \text{ kW/m}^2$ . It should be noted that external vessel cooling was considered only in the ANSYS simulation of thermo-mechanical behavior of the vessel wall. However, the external vessel cooling has an effect on the heat transfer in the melt pool also, which was not taken into account in this case. To assess the effect, we rerun the melt heat transfer problem for the 1.9 m pool case, taking into account the vessel cooling by changing external vessel temperature boundary conditions in the PECM analysis (see Figure 19b for a snapshot) and then performing the structural analysis with new temperature boundary conditions supplied by PECM. As shown in Figure 19b, we found that the wall normal heat flux settles to the level of about  $110 \text{ kW/m}^2$  except for one location y = 1.21 m which settles to the level of about  $200 \text{ kW/m}^2$  which means that all are well below the assumed CHF limit.

# Elmir L Forma Elmir L Delete Elmir L Forma Elmir L Delete

#### 3. Conclusions

We considered melt-vessel thermo mechanical interaction in a hypothetical severe accident in a Nordic Boiling Water Reactor with molten core materials relocated to the lower head and subsequent debris bed and melt pool formation. The melt inflicts thermal and mechanical loads which can induce creep leading to a mechanical failure of the reactor vessel wall. In this paper we considered melt pool configurations with depths of 0.7 m, 1.1 m, 1.5 m, and 1.9 m. A coupled thermo-mechanical creep analysis of each case reveals that if only CRGT cooling is activated then: (i) the case with 0.7 m and 1.1 m melt pool depths result in a ballooning type of vessel failure where creep strains are distributed in the lower section of the vessel that is covered by melt pool, and (ii) the case with 1.5 m, and 1.9 m melt pool depths result in a localized creep where creep strains are concentrated in the vicinity of the uppermost region of the melt pool. In the event of melt release, the consequences of these two modes of failure are different in terms of size of the breach, amount of melt which can be released at once, melt superheat, etc. Next, we investigated the possibility of in-vessel retention by an external vessel cooling that is implemented right before creep accelerates. In all melt pool configurations that are considered, we found that the external vessel cooling was able to suppress the creep and subsequently prevent the vessel failure.

#### 4. Acknowledgements

The work is supported by the Swedish Nuclear Radiation Protection Authority (SSM), Swedish Power Companies, European Commission (SARNET-2), Nordic Nuclear Safety

Program (NKS), and Swiss Federal Nuclear Safety Inspectorate (ENSI) under the APRI-MSWI program at the Royal Institute of Technology (KTH), Stockholm, Sweden.

#### 5. References

- [1] P. Kudinov, A. Karbojian, W. Ma, and T.-N. Dinh "The DEFOR-S Experimental Study of Debris Formation with Corium Simulant Materials", *Nuclear Technology*, 170(1), pp. 219-230 (2010).
- [2] P. Kudinov, A. Karbojian, C.-T. Tran, and W. Villanueva, "The DEFOR-A Experiment on Fraction of Agglomerated Debris as a Function of Water Pool Depth," *Proceedings of The 8th International Topical Meeting on Nuclear Thermal-Hydraulics, Operation and Safety (NUTHOS-8)*, Shanghai, China, October 10-14, N8P0296, (2010).
- [3] P. Kudinov and M. Davydov, "Development and Validation of the Approach to Prediction of Mass Fraction of Agglomerated Debris," *Proceedings of The 8th International Topical Meeting on Nuclear Thermal-Hydraulics, Operation and Safety (NUTHOS-8)*, Shanghai, China, October 10-14, N8P0298, (2010).
- [4] S. Yakush, P. Kudinov, and T.-N. Dinh, "Multiscale Simulations of Self-organization Phenomena in the Formation and Coolability of Corium Debris Bed," *Proceedings The 13th International Topical Meeting on Nuclear Reactor Thermal Hydraulics (NURETH-13)*, September 27-October 2, 2009. Kanazawa City, Ishikawa Prefecture, Japan, Paper N13P1143, (2009).
- [5] S. Yakush and P. Kudinov, "Effects of Water Pool Subcooling on the Debris Bed Spreading by Coolant Flow," *Proceedings of ICAPP 2011*, Nice, France, May 2-5, 2011, Paper 11416, 2011.
- [6] D. Magallon, K.H. Bang, S. Basu, G. Berthoud, M. Bürger, M.L. Corradini, H. Jacobs, O. Melikhov, K. Moriyama, M. Naitoh, J.H. Song, N. Suh, and T.G. Theofanous, "FCI phenomena uncertainties impacting predictability of dynamic loading of reactor structures (SERENA programme)," *Proceedings Workshop on Evaluation of Uncertainties in Relation to Severe Accidents and Level 2 Probabilistic Safety Analysis*, Hotel Aquabella, Aix-en-Provence, France, November 7–9 (2005).
- [7] T. G. Theofanous, C. Liu, S. Additon, S. Angelini, O. Kymäläinen, and T. Salmassi, *In-vessel coolability and retention of core melt*, DOE/ID-10460, Vol. 1-2, US DOE, October (1996).
- [8] H.-G. Willschuetz, E. Altstadt, B. R. Sehgal, and F.-P. Weiss, "Recursively coupled thermal and mechanical FEM-analysis of lower plenum creep failure experiments", *Annals of Nuclear Energy*, **33**, pp. 126-148 (2006).
- [9] K. Ikonen, "Mechanical analysis of Olkiluoto RPV bottom in core melting accident", VTT Research Report, PRO1/7017/04, 2004.
- [10] J. L. Rempe, S. A. Chavez, G. L. Thinnes, C. M. Allison, G. E. Korth, R. J. Witt, J. J. Sienicki, S. K. Wang, L. A. Stickler, C. H. Heath, and S. D. Snow, *Light Water Reactor Lower Head Failure*, Report NUREG/CR-5642, Idaho Falls (1993).
- [11] C.-T. Tran, T.-N. Dinh, "The effective convectivity model for simulation of melt pool heat transfer in a light water reactor pressure vessel lower head. Part I: Physical processes, modeling and model implementation", *Progress in Nuclear Energy*, **51**, pp. 849-859 (2009).
- [12] <a href="http://www.fluent.com/">http://www.fluent.com/</a>.
- [13] <a href="http://ansys.com/">http://ansys.com/</a>.
- [14] ANSYS 12.1, User's Manual, ANSYS<sup>®</sup>, Inc. (2009).
- [15] V. A. Bui and T.-N. Dinh, "Modeling of heat transfer in heated-generating liquid

- pools by an effective diffusivity-convectivity approach", *Proceedings of 2nd European Thermal-Sciences Conference*, Rome, Italy, 1365-1372 (1996).
- [16] U. Steinberner and H. H. Reineke, "Turbulent buoyancy convection heat transfer with internal heat sources", *Proceedings of the 6th International Heat Transfer Conference*, Toronto, Canada, 2, 305-310 (1978).
- [17] C.-T. Tran and T.-N. Dinh, "The effective convectivity model for simulation of melt pool heat transfer in a light water reactor lower head. Part II: Model assessment and application", *J. Progress in Nuclear Energy*, **51**, 860-871 (2009).
- [18] E. Andrade, "The viscous flow in metals and allied phenomena", *Proc. R. Soc. London A*, **84**, pp. 1-12 (1910).
- [19] K. Naumenko and H. Altenbach, *Modeling of Creep for Structural Analysis*, Springer-Verlag, Berlin, Germany (2007).
- [20] H. J. Frost and M. F. Ashby, *Deformation-Mechanism Maps: The Plasticity and Creep of Metals and Ceramics*, Pergamon, Oxford, UK (1982). <a href="http://engineering.dartmouth.edu/defmech">http://engineering.dartmouth.edu/defmech</a>.
- [21] W. Villanueva, C.-T. Tran, and P. Kudinov, "Coupled Thermo-Mechanical Creep Analysis for Boiling Water Reactor Pressure Vessel Wall Lower Head," *Proceedings of The 8th International Topical Meeting on Nuclear Thermal-Hydraulics, Operation and Safety (NUTHOS-8)*, Shanghai, China, October 10-14, N8P0248, (2010).
- [22] T. G. Theofanous, T.-N. Dinh, J. P. Tu, and A. T. Dinh, "The boiling crisis phenomenon. Part II: dryout dynamics and burnout", *Exp. Therm. and Fluid Sci.*, **26**, pp. 793-810 (2002).
- [23] S. Angelini, J. P. Tu, Y. A. Buyevich, and T. G. Theofanous, "The mechanism and prediction of critical heat flux in inverted geometries", *Nucl. Eng. Des.*, **200**, pp. 83-94 (2000).